Chinese Chemical Letters 33 (2022) 812–816

Contents lists available at ScienceDirect

Chinese Chemical Letters

journal homepage: www.elsevier.com/locate/cclet

Enhanced photocatalytic CO_2 hydrogenation with wide-spectrum utilization over black TiO_2 supported catalyst

Binbin Jin[a], Xin Ye[a], Heng Zhong[a,b,c], Fangming Jin[a,b,c,*], Yun Hang Hu[d,*]

[a] School of Environmental Science and Engineering, State Key Lab of Metal Matrix Composites, Shanghai Jiao Tong University, Shanghai 200240, China
[b] Center of Hydrogen Science, Shanghai Jiao Tong University, Shanghai 200240, China
[c] Shanghai Institute of Pollution Control and Ecological Security, Shanghai 200092, China
[d] Department of Materials Science and Engineering, Michigan Technological University, Houghton, Michigan 49931-1295, United States

ARTICLE INFO

Article history:
Received 8 June 2021
Revised 29 June 2021
Accepted 20 July 2021
Available online 30 July 2021

Keywords:
Photothermal
Black TiO_2
CO_2
Electron-rich
Hydrogenation

ABSTRACT

Light-driven conversion of CO_2 into chemicals/fuels is a desirable approach for achieving carbon neutrality using clean and sustainable energy. However, its scale-up application is restricted due to insufficient efficiency. Herein, we present a photothermal catalytic hydrogenation of CO_2 into CH_4 over Ru/black TiO_2 catalysts, aiming to achieve the synergistic use of light and heat in solar energy during CO_2 conversion. Owing to the desirable spectral response ability and photothermal conversion performance of black TiO_2, an efficient combination of photocatalysis and thermocatalysis has been established. The CO_2 hydrogenation was significantly accelerated because of the increased catalyst surface temperature enabled by the photothermal effect of black TiO_2. Simultaneously, through the *in situ* X-ray photoelectron spectroscopy (XPS) observation, electron-rich Ru nanoparticles was achieved based on the photo-induced excitation, thereby providing more negative hydride to improve nucleophilic attack to the CO_2, obtaining the CH_4 yield of 93.8%.

To alleviate the climate change caused by carbon cycle imbalance and reduce the dependence on fossil fuels, conversion of CO_2 into value added chemicals and fuels is one promising choice [1-4]. Considering that solar energy is clean and inexhaustible to a certain extent, photocatalysis is thought to play a crucial role in the future industry system and has been widely investigated [5,6]. Thus, photocatalytic CO_2 conversion is a desirable approach for CO_2 utilization. However, insufficient efficiency limits the application of photocatalytic CO_2 conversion in large-scale industrial production. Although various strategies have been applied to improve the photocatalytic performance, the efficient CO_2 conversion is still a vital challenge.

Photothermal catalysis, which has the potential to utilize the whole solar spectrum, is one desirable choice for this issue [7,8]. During the photothermal catalysis, while the short-wavelength light could be converted into photogenerated electron-hole pairs to drive the photochemical reactions, the long-wavelength light could be converted into heat, accelerating the reaction, especially for the surface endothermic reaction [9,10]. Considering the high efficiency of thermochemical method, the combination of photocatalysis and thermocatalysis could strike a balance between energy consumption and conversion efficiency, which has a broad application prospect in CO_2 methanation [11-15].

To achieve desirable synergy between photochemical and thermochemical, the construction design of catalyst is crucial. TiO_2 has been widely applied in photocatalysis [16,17]. However, the photocatalytic activity of TiO_2 is greatly limited due to its poor response ability to visible light [18,19]. To solve this issue, Chen *et al.* prepared TiO_{2-x} (black TiO_2) from TiO_2 by strong reduction treatment, and black TiO_2 exhibits excellent spectral response range and photocatalytic activity [20,21]. Thus, black TiO_2 has attracted increasing attention and been widely applied in photocatalysis such as photocatalytic water splitting. Additionally, because of its inherent black color, black TiO_2 could perform high photothermal conversion ability. Considering the broad spectral response range and excellent photothermal conversion efficiency of black TiO_2 [22-25], it is reasonable to speculate that black TiO_2 could balance the photoelectric conversion and photothermal conversion during the photothermal catalytic CO_2 conversion, giving promising catalytic activity. Therefore, in the present work, supported black TiO_2 was synthesized for light-driven catalytic hydrogenation of CO_2 to CH_4 using ruthenium as the active metal, and the synergic mechanism between photocatalysis and thermocatalysis in the CO_2 conversion was investigated.

* Corresponding authors.
E-mail addresses: fmjin@sjtu.edu.cn (F. Jin), yunhangh@mtu.edu (Y.H. Hu).

https://doi.org/10.1016/j.cclet.2021.07.046
1001-8417/

Table 1
The CH_4 yield from catalytic conversion of CO_2 over different catalysts (reaction conditions: 0.4 MPa mixture gas-N_2:H_2:CO_2 = 4:5:1, 20 mg catalyst, 1 h).

Entry	Catalyst	Yield of CH_4 (%)[a]	Yield of CH_4 (%)[b]	Yield of CO (%)[c]
1	TiO_2	ND	ND	ND
2	Black TiO_2	ND	ND	ND
3	2 wt% Ru/TiO_2	ND	18.7	0.1
4	2 wt% Ru/black TiO_2	ND	40.1	0.2
5[c]	2 wt% Ru/black TiO_2	ND	ND	ND

ND = not detected.
[a] Without light.
[b] With light.
[c] Without CO_2.

Firstly, as shown in Table 1, no CH_4 was detected in all entries without irradiation. Considering the high thermodynamic stability of CO_2, it is difficult to drive the hydrogenation of CO_2 without additional energy input at low temperature. Subsequently, the introduction of irradiation brought significant increase in CH_4 yield (Table 1, entries 3 and 4). Most importantly, the CH_4 yield achieved over 2 wt% Ru/black TiO_2 under irradiation was 40.1%, which was 2 times higher than that achieved over 2 wt% Ru/TiO_2. Additionally, small amount of CO was also produced in entries 3 and 4. CO species are commonly considered as the important intermediate during the CO_2 hydrogenation. Additionally, we performed the experiments without CO_2 and no carbon containing products were detected, indicating that the injected CO_2 is the sole carbon source. There are two possible reasons for the remarkable improvement of the catalytic activity of Ru/black TiO_2: (1) The enhancement of CO_2 adsorption capacity; (2) the improvement of spectral response capacity and photothermal conversion efficiency. In order to verify the above conjectures, the CO_2 adsorption capacity and spectral response ability of the catalysts were investigated, and the photothermal conversion performances of the catalysts were evaluated.

Firstly, the light response characteristics of the prepared materials were investigated and Fig. 1a shows the UV-vis diffuse reflectance spectra (DRS) of TiO_2 and black TiO_2. The spectral response ability of black TiO_2 in long wavelength range is much higher than that of TiO_2. It is possible that, after the hydrogenation at high temperature, the intrinsic symmetry of TiO_2 crystal was broken, forming an amorphous shell on the TiO_2 surface [26,27]. Thus, a secondary narrow bandgap would be introduced into TiO_2, enhancing the light absorption. Additionally, considering the more significant thermal effect of long wavelength light, the enhanced long wavelength light response ability of black TiO_2 can make black TiO_2 perform better photothermal conversion efficiency under the broad wavelength irradiation. Subsequently, the CO_2 adsorption observation was conducted. As shown in Fig. S1 (Supporting information), the CO_2 adsorption amount of both TiO_2 and black TiO_2 increased with the increase of pressure and the CO_2 adsorption ability of black TiO_2 was better than that of TiO_2. The enhanced CO_2 adsorption ability of black TiO_2 gives the prepared catalysts better catalytic activity. Furthermore, nitrogen adsorption/desorption isotherms of TiO_2 and black TiO_2 were compared. The Brunauer-Emmett-Teller (BET) specific surface areas of TiO_2 and black TiO_2 are 99.8 m^2/g and 100.1 m^2/g, respectively (Figs. S2a and b in Supporting information). The hydrogenation treatment has not brought significant change of specific surface area to black TiO_2. Thus, it is reasonable to speculate that the enhanced CO_2 adsorption capacity can be attributed to the formation of oxygen vacancy in black TiO_2 [28,29].

Then, the textural properties were characterized by X-ray diffraction (XRD). As shown in Fig. 1b, the XRD patterns of the catalysts displayed no obvious differences in crystal form compared to the original TiO_2. However, it is worth noting that the peak intensity of black TiO_2 is significantly lower than that of TiO_2 and the

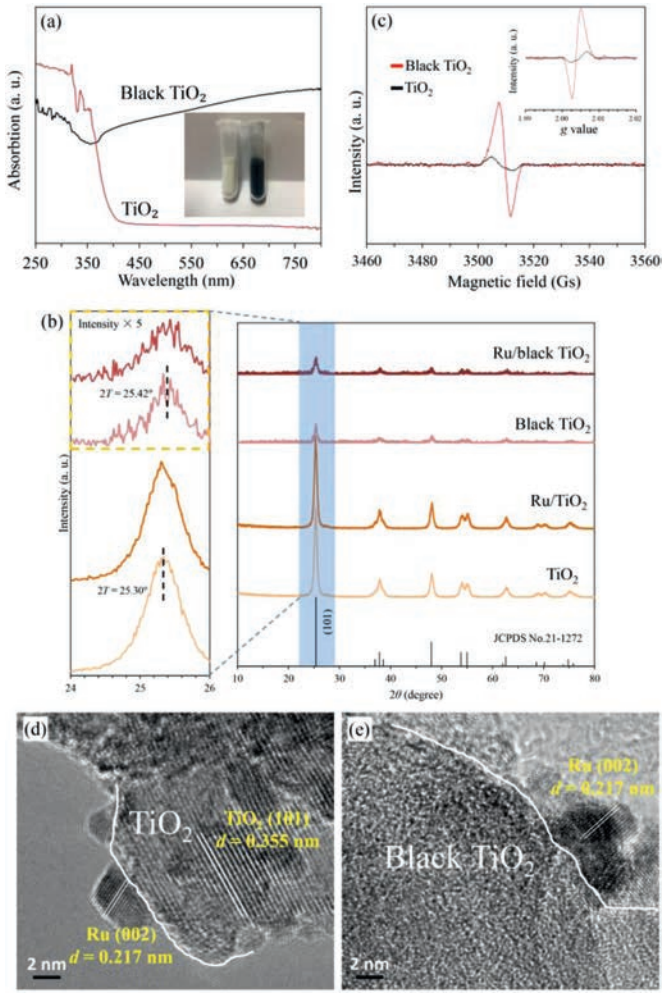

Fig. 1. (a) UV-vis DRS of TiO_2 and black TiO_2. (b) XRD patterns of TiO_2, black TiO_2, 2 wt% Ru/TiO_2 and 2 wt% Ru/black TiO_2. (c) EPR spectra of TiO_2 and black TiO_2. (d, e) HRTEM images of 2 wt% Ru/TiO_2 and 2 wt% Ru/black TiO_2.

(101) plane characteristic peak of black TiO_2 shifts to larger diffraction angle, which can be owing to the decrease of the intrinsic material crystallinity and formation of lattice defects [30]. Subsequently, X-ray photoelectron spectroscopy analysis was applied to investigate the 2 wt% Ru/black TiO_2 (Figs. S3 and S4 in Supporting information). In the XPS diagram of O 1s (Fig. S4), it can be seen that the O 1s can be divided into two peaks, among which the peak at 529.52 eV is attributed to the lattice oxygen (O_L), while the peak at 530.73 eV can be attributed to the oxygen vacancy (O_V) in black TiO_2 [31,32]. During the high temperature reduction of TiO_2, part of the oxygen atoms were deprived, causing the decrease of the electron cloud density and thereby increasing the binding energy of O 1s. Additionally, the existence of oxygen vacancies was proved by electron paramagnetic resonance (EPR) measurements. As shown in Fig. 1c, a strong EPR signal (centering at $g = 2.003$) can be observed in black TiO_2 EPR spectra while TiO_2 only exhibits an extremely weak EPR signal [33]. It indicates that lots of oxygen vacancies were produced in black TiO_2, which accords with the XPS analysis results.

To further investigate the morphology and structure of the catalysts, high-resolution transmission electron microscopy (HRTEM) were conducted. The measured average particle sizes of TiO_2 and black TiO_2 are 22.5 ± 3.0 nm and 28.1 ± 4.7 nm, respectively (Fig. S5 in Supporting information). The agglomeration of the catalysts after calcination at high temperature is one possible reason

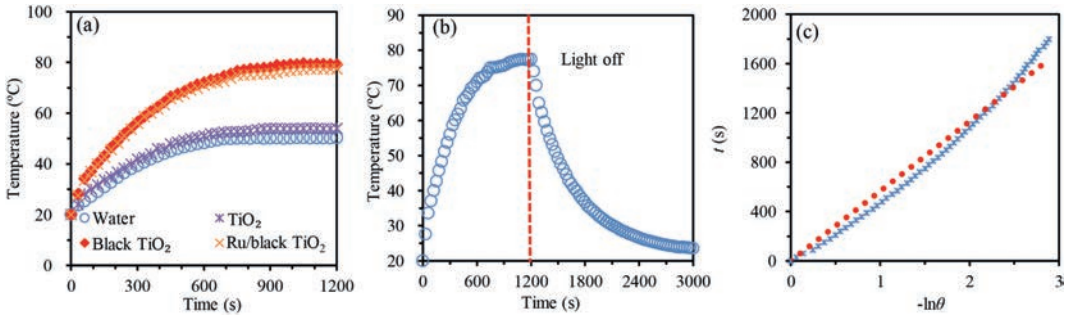

Fig. 2. (a) Temperature curves of pure water, TiO_2, black TiO_2 and 2 wt% Ru/black TiO_2 aqueous solution (200 μg/mL) under irradiation. (b) The temperature curve of the 2 wt% Ru/black TiO_2 aqueous solution (200 μg/mL) for 3000 s. (c) Linear time data versus -lnθ obtained from the cooling period.

for the increase of average particle size. Additionally, as shown in Figs. 1d and e, Ru nanoparticles in the 2 wt% Ru/TiO_2 and 2 wt% Ru/black TiO_2 catalysts are loaded on the support surface in the form of small particle and the contact interface between Ru and support can be clearly observed. The lattice fringes belonged to the Ru (002) crystal facet are clearly observed [34]. Owing to the well-contacted interface, efficient photogenerated carriers transferring can be constructed during the reaction. In addition, the lattice fringes of TiO_2 in 2 wt% Ru/TiO_2 catalyst are orderly arranged, and the lattice spacing is 0.355 nm, belonging to (101) crystal facet of anatase TiO_2 [35]. However, it is difficult to observe continuous lattice fringes in 2 wt% Ru/black TiO_2. The removal of O during reduction treatment broke the stoichiometric balance of TiO_2, forming amorphous phase [20,36]. This result also agrees with the XRD analysis result that the crystallinity of black TiO_2 has been weakened structurally.

As aforementioned that the increase of catalytic activity of Ru/black TiO_2 can also be attributed to the enhanced photothermal conversion ability, therefore, the photothermal conversion performances of Ru/TiO_2 and Ru/black TiO_2 were compared. Firstly, surface temperatures of the prepared catalysts under irradiation were directly observed based on IR temperature measuring device. As shown in Fig. S6 (Supporting information), the rising rate of the surface temperature of 2 wt% Ru/black TiO_2 was significantly higher than that of 2 wt% Ru/TiO_2 under irradiation. After 300 s, the surface temperature of 2 wt% Ru/black TiO_2 reached 283.7 °C, while the temperature of 2 wt% Ru/TiO_2 was only 223.1 °C. It can be seen from Fig. S7 (Supporting information) that the overall temperature of reaction system raised gradually during the reaction due to the photothermal conversion effect of the catalyst.

Furthermore, the photothermal conversion efficiency of 2 wt% Ru/black TiO_2 was evaluated. The materials were dispersed in aqueous solution with water as the negative control. Initial temperature of the solution and room temperature were controlled at 20 °C. The solutions were irradiated under the Xe lamp and the lamp was turned off after 1200 s, and the temperature change was observed for 3000 s (Figs. 2a and b). The highest temperature of 2 wt% Ru/black TiO_2 aqueous solution is 79.6 °C while the temperature of TiO_2 aqueous solution is only 53.8 °C (Fig. 2a). It is worth noting that the highest temperature of 2 wt% Ru/black TiO_2 solution is slightly lower than that of black TiO_2. Considering that near-infrared (NIR) absorption ability has marked impact on photothermal conversion [37], UV-vis-NIR DRS of the catalysts were conducted. As shown in Fig. S8, TiO_2 displays poor NIR response and the loading of Ru improve its NIR absorption. However, there is no significant difference between the spectra of black TiO_2 and Ru/black TiO_2, which means that the intrinsic NIR absorption of black TiO_2 is higher than that of Ru NPs. Therefore, the photothermal conversion capacity of black TiO_2 is slightly higher than that of Ru/black TiO_2. The photothermal conversion efficiency (η) can

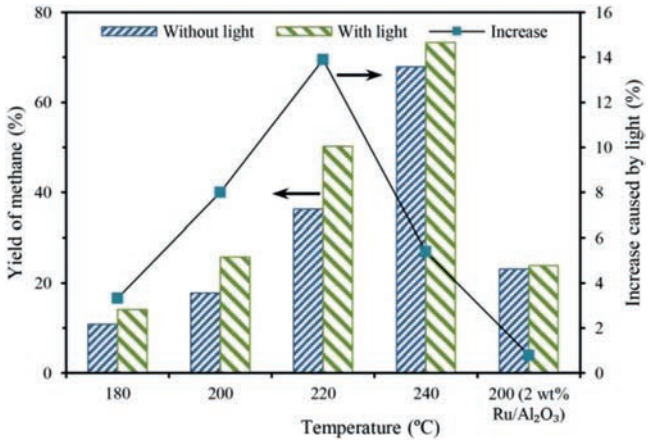

Fig. 3. The yield of CH_4 from catalytic conversion of CO_2 at different temperatures (reaction conditions: 0.4 MPa mixture gas-N_2:H_2:CO_2 = 4:5:1, 20 mg 2 wt% Ru/black TiO_2, 1 h, 100 mW/cm^2).

be calculated based on Eq. 1 [37-39]:

$$\eta = \frac{hA(\Delta T_{max,mix} - \Delta T_{max,H_2O})}{I} \quad (1)$$

where h, A, I, $\Delta T_{max,mix}$ and $\Delta T_{max,H_2O}$ represent the heat transfer coefficient, the container surface area, the total energy Ru/black TiO_2 nanoparticles absorbed, the temperature change of the 2 wt% Ru/black TiO_2 suspension and water at the maximum stable temperature, respectively. Based on the fitting parameters of the cooling period in Fig. 2c, the η value of 2 wt% Ru/black TiO_2 is calculated to be 37.9%. The calculation details can be seen in the Supporting Information. Owing to the efficient photothermal conversion based on black TiO_2, strong heat center can be produced on the catalyst surface under irradiation, improving the substances (CO_2 and H_2) activation and accelerating the reaction [40].

Subsequently, to verify the participation of photogenerated carriers during the CO_2 conversion, the irradiation intensity was decreased to 1 sun (100 mW/cm^2) and a series of experiments at different temperatures were conducted. The experiments were carried out at 180, 200, 220 and 240 °C, respectively. As shown in Fig. 3, the methane yield increased with the increase of temperature, which indicates that the increase of reaction temperature is conducive to the methanation of CO_2. Most importantly, the CH_4 yields increased at all temperatures after the introduction of light and highest synergy was obtained at 220 °C, which means that intrinsic excitation process of the catalysts may played an important role during the reaction.

Considering the large band gap of Al_2O_3, Ru/Al_2O_3 was prepared to avoid the excitation of catalyst and its catalytic performance was observed to further confirm the effect of photogener-

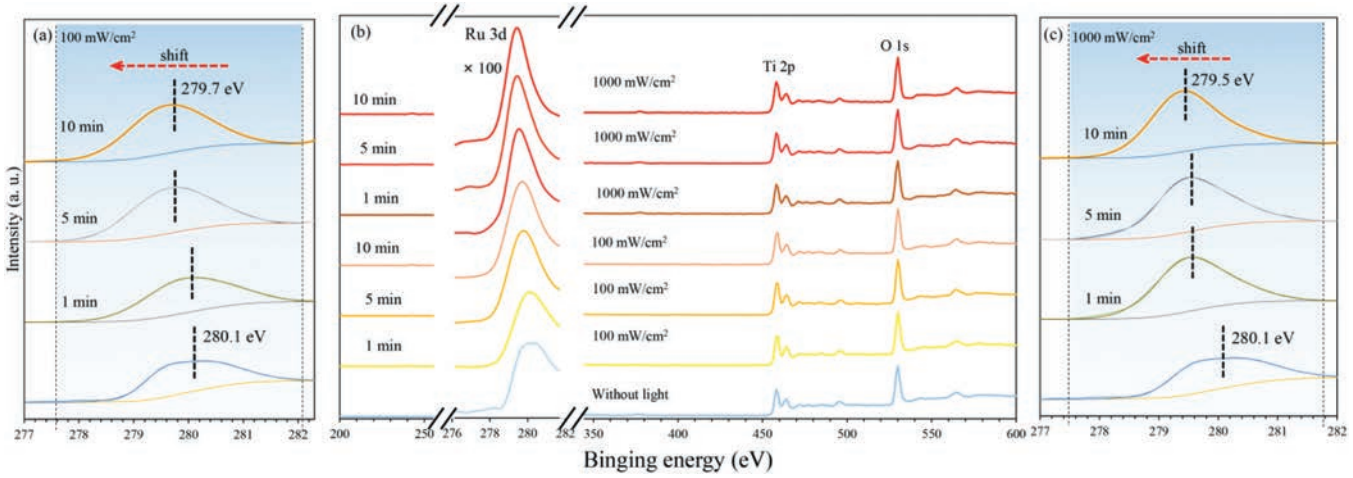

Fig. 4. *In situ* high-resolution XPS spectrum of 2 wt% Ru/black TiO_2. (a) Ru $3d_{5/2}$ of 2 wt% Ru/black TiO_2 obtained under irradiation (100 mW/cm^2); (b) survey spectrum; (c) Ru $3d_{5/2}$ of 2 wt% Ru/black TiO_2 obtained under irradiation (1000 mW/cm^2).

ated carriers. As displayed in the Fig. 3, the CH_4 yield showed no significant increase over Ru/Al_2O_3 after the introduction of light. Thus, it is reasonable to speculate that, during the hydrogenation of CO_2 over Ru/black TiO_2, not only the heat input generated from photothermal conversion but also the photogenerated carriers promote the conversion of CO_2. The role photogenerated carriers played during CO_2 conversion were investigated in mechanism discussion section.

According to the above results and the reported CO_2 hydrogenation mechanism, the functionary mechanism of photogenerated carrier was proposed (Fig. S9 in Supporting information). Due to the low Fermi level of Ru and the well-contacted interface between Ru nanoparticle and black TiO_2 nanoparticle (Fig. 1f), it is reasonable to speculate that the photogenerated electrons would be gathered in Ru nanoparticles, forming electron-rich Ru surface. Furthermore, to monitor the electron density variation of Ru nanoparticles, *in situ* high-resolution XPS was carried out. As displayed in Fig. 4, the binding energy of Ru $3d_{5/2}$ shows a significant decrease after the introduction of light. In addition, with the gradual increase of irradiation intensity and irradiation time, the binding energy of Ru $3d_{5/2}$ displayed a further shifting tendency.

Considering that the increase of electron density can enhance the shielding effect of electron clouds, which would decrease the binding energy of Ru 3d core level, it is reasonable to speculate that an electron injection process is achieved during the reaction. In contrast, the introduction of light caused the increase of O 1s binding energy (Fig. S10 in Supporting information), indicating that oxygen is in electron deficient state, which could be owing to the photogenerated holes. It is worth noting that the activation of H_2 is essential for the CO_2 hydrogenation. The formation of electron-rich Ru surface can provide more negative hydride, thus enhancing the nucleophilic attack reactivity of the hydride to the carbon center of CO_2 [41,42]. Besides, the light with larger wavelength could be converted into heat due to the photothermal conversion, further improving the CO_2 conversion. It is one promising way to achieve efficient hydrogenation of CO_2 using light as the only driving force based on the synergy between photocatalysis and thermocatalysis.

Additionally, a series of Ru/black TiO_2 catalysts with different Ru loading amount were prepared and the circulation stability test was carried out. The CH_4 yield increased with the increase of Ru loading amount and 93.8% of CH_4 yield was achieved within 2 h over 5 wt% Ru/black TiO_2 (Fig. S11 in Supporting information). The H_2-temperature programmed desorption (TPD) was carried out to investigate the adsorption strength between the adsorbed hydrogen and catalysts. As displayed in Fig. S12 (Supporting information), all tested catalysts displayed two significant hydrogen desorption peaks. The desorption peaks around 270 °C could be ascribed to the weakly adsorbed hydrogen on Ru surface and the peaks at high temperature (around 340 °C) could be ascribed to the strongly adsorbed hydrogen on the surface of black TiO_2 caused by hydrogen spillover [43-45]. Such spillover could do contribution to the hydrogenation of CO_2. Additionally, no significant decrease in CH_4 yield was observed during the stability test of 5 wt% Ru/black TiO_2 (Fig. S13 in Supporting information). The XRD patterns of the collected catalysts after stability test display similar XRD patterns (Fig. S14 in Supporting information) and no high temperature phases such as rutile TiO_2 were produced after reaction, indicating that the catalyst can maintain desirable stability under the current reaction conditions.

In summary, a black TiO_2 supported catalyst was constructed for the photothermal catalytic CO_2 hydrogenation. Owing to the introduction of oxygen vacancies, the CO_2 adsorption ability of the black TiO_2 supported catalyst was significantly enhanced, improving the CO_2 conversion. The wide spectral response range and high photothermal conversion efficiency of black TiO_2 brought desirable catalytic performance for photocatalytic hydrogenation of CO_2 to the prepared Ru/black TiO_2. Additionally, based on the well-contacted interface between Ru nanoparticle and black TiO_2 nanoparticle, an electron injection process was achieved to form electron-rich Ru metal nanoparticles, further improving the hydrogenation of CO_2. This study opens the step for full wavelength range utilization of solar energy in light-driven conversion of CO_2.

Declaration of competing interest

The authors declare that they have no known competing financial interests or personal relationships that could have appeared to influence the work reported in this paper.

Acknowledgments

The authors gratefully acknowledge the support from the National Natural Science Foundation of China (No. 21978170), the National Key R&D Program of China (No. 2017YFC0506004), the Natural Science Foundation of Shanghai (No. 19ZR1424800), and the Center of Hydrogen Science, Shanghai Jiao Tong University, China.

Supplementary materials

Supplementary material associated with this article can be found, in the online version, at doi:10.1016/j.cclet.2021.07.046.

References

[1] J. Albero, Y. Peng, H. Garcia, ACS Catal. 10 (2020) 5734–5749.
[2] M. Aresta, A. Dibenedetto, A. Angelini, Chem. Rev. 114 (2014) 1709–1742.
[3] K. Li, B. Peng, T. Peng, ACS Catal. 6 (2016) 7485–7527.
[4] Z. Jiang, H. Sun, T. Wang, et al., Energy Environ. Sci. 11 (2018) 2382–2389.
[5] W. Wang, G. Li, D. Xia, et al., Environ. Sci. 4 (2017) 782–799 Nano.
[6] W. Wang, T. An, G. Li, et al., Appl. Catal. B 217 (2017) 570–580.
[7] L.B. Hoch, P.G. O'Brien, A. Jelle, et al., ACS Nano 10 (2016) 9017–9025.
[8] J.C. Kennedy, A.K. Datye, J. Catal. 179 (1998) 375–389.
[9] X. Meng, T. Wang, L. Liu, et al., Angew. Chem. Int. Ed. 53 (2014) 11478–11482.
[10] L. Wang, Y. Dong, T. Yan, et al., Nat. Commun. 11 (2020) 2432.
[11] M. Ghoussoub, M. Xia, P.N. Duchesne, D. Segal, G. Ozin, Energy Environ. Sci. 12 (2019) 1122–1142.
[12] Y. Li, J. Hao, H. Song, et al., Nat. Commun. 10 (2019) 2359.
[13] Z. Li, R. Shi, J. Zhao, T. Zhang, Nano Res. 14 (2021) 4828–4832.
[14] N.T. Nguyen, M. Xia, P.N. Duchesne, et al., Nano Lett. 21 (2021) 1311–1319.
[15] Z. Li, J. Liu, R. Shi, G.I.N. Waterhouse, X. Wen, T. Zhang, Adv. Energy Mater. 11 (2021) 2002783.
[16] S.N. Habisreutinger, L. Schmidt-Mende, J.K. Stolarczyk, Angew. Chem. Int. Ed. 52 (2013) 7372–7408.
[17] D. Mateo, J. Albero, H. Garcia, Joule 3 (2019) 1949–1962.
[18] X. He, A. Wang, P. Wu, et al., Sci. Total Environ. 743 (2020) 140694.
[19] M. Nemiwal, T. Zhang, D. Kumar, Sci. Total Environ. 767 (2021) 144896.
[20] X. Chen, L. Liu, P.Y. Yu, S.S. Mao, Science 331 (2011) 746–750.
[21] X. Chen, L. Liu, F. Huang, Chem. Soc. Rev. 44 (2015) 1861–1885.
[22] Y.H. Hu, Angew. Chem. Int. Ed. 51 (2012) 12410–12412.
[23] A. Naldoni, M. Allieta, S. Santangelo, et al., J. Am. Chem. Soc. 134 (2012) 7600–7603.
[24] W. Zhou, W. Li, J.Q. Wang, et al., J. Am. Chem. Soc. 136 (2014) 9280–9283.
[25] A. Naldoni, M. Altomare, G. Zoppellaro, et al., ACS Catal. 9 (2019) 345–364.
[26] X. Lu, A. Chen, Y. Luo, et al., Nano Lett. 16 (2016) 5751–5755.
[27] T.D. Nguyen, J. Li, E. Lizundia, et al., Adv. Funct. Mater. 29 (2019) 1904639.
[28] Z. Geng, X. Kong, W. Chen, et al., Angew. Chem. Int. Ed. 57 (2018) 6054–6059.
[29] J. Ye, C. Liu, D. Mei, Q. Ge, ACS Catal. 3 (2013) 1296–1306.
[30] L. Pan, M. Ai, C. Huang, et al., Nat. Commun. 11 (2020) 418.
[31] Q. Wang, W. Wang, L. Zhong, et al., Appl. Catal. B 220 (2018) 290–302.
[32] C. Xu, W. Huang, Z. Li, et al., ACS Catal. 8 (2018) 6582–6593.
[33] H. Song, C. Li, Z. Lou, Z. Ye, L. Zhu, ACS Sustain. Chem. Eng. 5 (2017) 8982–8987.
[34] X. Gao, S. Zhu, M. Dong, J. Wang, W. Fan, Appl. Catal. B 259 (2019) 118076.
[35] X. Lin, K. Yang, R. Si, et al., Appl. Catal. B 147 (2014) 585–591.
[36] T. Jedsukontorn, T. Ueno, N. Saito, M. Hunsom, J. Alloys Compd. 726 (2017) 567–577.
[37] Y. Liu, K. Ai, J. Liu, et al., Adv. Mater. 25 (2013) 1353–1359.
[38] D.K. Roper, W. Ahn, M. Hoepfner, J. Phys. Chem. C 111 (2007) 3636–3641.
[39] Q. Zou, M. Abbas, L. Zhao, et al., J. Am. Chem. Soc. 139 (2017) 1921–1927.
[40] M. Cai, C. Li, L. He, Rare Met. 39 (2020) 881–886.
[41] X. Lv, G. Lu, Z. Wang, Z. Xu, G. Guo, ACS Catal. 7 (2017) 4519–4526.
[42] Q. Liu, X. Yang, L. Li, et al., Nat. Commun. 8 (2017) 1407.
[43] X. Wang, P. Wu, Z. Wang, et al., ACS Sustainable Chem. Eng. 9 (2021) 3083–3094.
[44] R. Prins, Chem. Rev. 112 (2012) 2714–2738.
[45] Z. Wu, Y. Mao, X. Wang, M. Zhang, Green Chem. 13 (2011) 1311–1316.